Template Synthesis

DOI: 10.1002/anie.201407005

Supramolecular Transcription of Guanosine Monophosphate into Mesostructured Silica**

Carlos J. Bueno-Alejo, Luis A. Villaescusa, and Alfonso E. Garcia-Bennett**

Abstract: *There is large interest in replicating biological supramolecular structures in inorganic materials that are capable of mimicking biological properties. The use of 5-guanosine monophosphate in the presence of Na^+ and K^+ ions as a supramolecular template for the synthesis of well-ordered mesostructured materials is reported here. Mesostructured particles with the confined template exhibit high structural order at both meso- and atomic scales, with a lower structural symmetry in the columnar mesophase. Although a chiral space group can not be deduced from X-ray diffraction, analysis by electron microscopy and circular dichroism confirms a chiral stacking arrangement along the c-axis. Guanosine monophosphate based mesophases thus illustrate the possibility for specific molecular imprinting of mesoporous materials by genetic material and the potential for higher definition in molecular recognition.*

The self-assembly of guanosine-based nucleosides into supramolecular quadruplex (G) structures plays a fundamental function in a variety of biological processes. Guanosine derivatives are involved in intracellular signal transduction and have been identified in repetitive genomic sequences in telomeres, in ribosomal DNA, immunoglobulin heavy-chain switch regions, and in the control regions of proto-oncogenes.[1] Guanosine monophosphate (GMP) is a nucleotide monomer in messenger RNA, and is a reference for the structural study of G4 quartets.[2,3] There is also large interest in the replication of the biological functions of nucleosides within inorganic materials, as these may offer novel material properties such as molecular recognition, and selective ion transport for advanced targeting in nanomedicine.[4]

The GMP template is composed of guanine, ribose, and phosphate moieties. The phosphate groups reside on the exterior of the G4 columns and prevent the tetrameric units from stacking in register, rotating each tetramer by 30° and thereby inducing a chiral arrangement along the column. In solution at neutral pH, GMP monomers exist in two conformations, C2′-*endo* and C3′-*endo* (Figure 1), which result in two different types of tetramer arrangements and a right-handed 5-GMP helix.[5] The self-assembly of 5-GMP relies on Hoogsteen-type hydrogen bonding between four GMP molecules, which form tetramers. Subsequent π-stacking interactions between adjacent tetramers promote the formation of columnar phases (Col_{hex}), which are further stabilized by small cations (Na^+, K^+, Rb^+, Sr^{2+}).[6] We report here the cooperative self-assembly of 5-GMP and the silica precursors 3-aminopropyltriethoxysilane (APES) and tetraethyl orthosilicate (TEOS) to generate ordered mesostructured materials through a recently developed approach.[7,8] A favorable electrostatic interaction between a variety of supramolecular templates and silica precursors can be achieved by using carboxylate moieties and positively charged amino propyltriethoxysilane, which acts as a suitable co-structure directing agent for the formation of mesostruc-

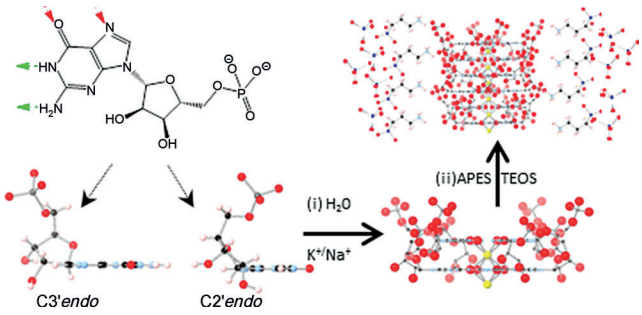

Figure 1. Molecular representation of 5-guanosine monophosphate molecules in solution, showing the C2′-*endo* and C3′-*endo* forms at neutral pH and their self-assembly into chiral tetrameric columnar structures through alternate layers of N- and S-type tetramers in the presence of M^+ ions.[5] Red: O, light blue: N, black: C, white: H, gray: P, bright yellow: K, dark blue: Si. The guanine moiety is capable of hydrogen bonding to form each tetramer (marked by arrows), whilst the phosphate moiety is capable of electrostatic interaction with two positively charged APES molecules.

[*] Dr. C. J. Bueno-Alejo, Dr. L. A. Villaescusa[+]
Centro de Reconocimiento Molecular y Desarrollo (IDM), UPV-UV
Camino de Vera, 46022 Valencia (Spain)
Dr. L. A. Villaescusa[+]
Departamento de Química and CIBER de Bioingeniería
Biomateriales y Nanomedicina (CIBER-BBN)
Universidad Politécnica de Valencia
Camino de Vera, 46022 Valencia (Spain)
E-mail: lvillaes@qim.upv.es
Dr. A. E. Garcia-Bennett[+]
Department of Materials and Environmental Chemistry
Arrhenius Laboratory, Stockholm University
10691 Stockholm (Sweden)
E-mail: alfonso@mmk.su.se
[+] These authors contributed equally to this work.

[**] This work was supported by the Swedish Research Council (A.E.G.B.), and L.A.V. thanks the Spanish Government for financial support (project MAT2012-38429-C04) and D.E.L.I for help with the ICP/MS analysis. We are grateful to Prof. Sven Hovmoller (Stockholm University) for advice and helpful discussions regarding electron crystallography and CRISP. We are indebted to Dr. Isabel Correia (Technical University of Lisbon) for her help with circular dichroism measurements.

Supporting information for this article is available on the WWW under http://dx.doi.org/10.1002/anie.201407005.

tured materials.[8,9] To promote the electrostatic interaction between the phosphate group of 5-GMP and the amino group in APES, an aqueous solution of Na_2GMP and KCl was prepared (see Experimental Section). To this was added APES followed by HCl (37%) and the silica source (TEOS). The solid was collected after two hours at room temperature by filtration, and dried. Powder X-ray diffraction (XRD) reveals the mesostructured sample (denoted *a*NGM-1, nanoporous guanosine material) has good crystallinity, as judged by the high Miller indexes that can be observed up to the (400) reflection, assuming a hexagonal crystal class (Figure 2).[10] Apart from the mesoscale order, two additional

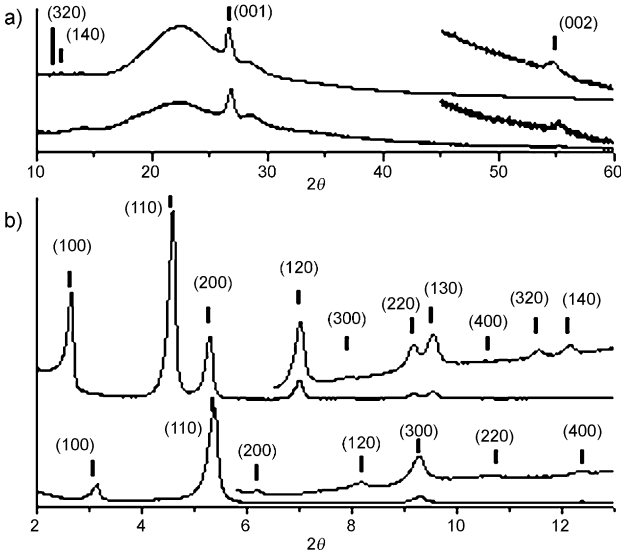

Figure 2. a) High- and b) low-angle XRD patterns of *a*NGM-1 (bottom) and hydrothermally treated *h*NGM-1 (top) samples. The insets show enlarged regions of the mesoscale order. The patterns are indexed on the basis of a 3D hexagonal unit cell. Note that high-angle peaks associated with the [001] direction can be distinguished. The *y*-axis represents intensity in arbitrary units.

sharp reflections can be distinguished at higher Bragg angles, which are related to the ordering along the *c*-axis. A peak at approximately 3.4 Å, typical of discotic liquid crystals, can be clearly discerned and is due to the stacking repeat distance of the GMP tetramers.[11] Within a 3D hexagonal system, this peak is indexed as the (001) reflection. The small broad shoulder next to this reflection corresponds to the *hk1* family of planes. Another diffraction peak is centered at 55° (1.67 Å), which is indexed as (002). According to the tentatively assigned hexagonal structure, *a*NGM-1 exhibits a unit cell with parameters $a = 32.8$ and $c = 3.4$ Å.

Analysis of the solid by a number of techniques, including ^{1}H NMR spectroscopy after dissolution in $NaOD/D_2O$ as well as thermogravimetric and chemical analysis of alkaline cations (see Figures S1–S3 in the Supporting Information), yields a composition of $4\,GMP : 7.66\,SiO_{3/2}(CH_2)_3NH_2 : 11.4\,SiO_2 : 0.18\,Na_2O : 0.69\,K_2O : 39.54\,H_2O$. The absence of signals corresponding to ethanol in the ^{1}H NMR spectrum indicates that TEOS is fully hydrolyzed during the synthesis. The GMP/APES ratio for *a*NGM-1 is approximately 2:1, thus suggesting an electrostatic interaction between the doubly negative charged phosphate and the protonated amines of the APES. This is consistent with the formation of a supramolecular lining of silica from APES surrounding the GMP tetramers, whose further enrichment with silica during the synthesis produces the columnar mesophase. An excess of alkaline cations in the composition with respect to the amount necessary to fully occupy the intertetramer sites is noted, probably balancing the SiO^- species within the silica wall. Also, there is around three times more potassium than sodium cations, with $K^+/GMP = 0.35{:}1$.

Previous measurements conducted in solution indicate that K^+ ions preferentially occupy the intertetramer sites, and thus increase the self-association constant significantly.[12–14] To confirm this in the present system, we varied the composition of the starting alkaline cation, which led to variations in the relative intensities and positions of the high-angle diffraction peaks (see Figure S4 in the Supporting Information). When only Na^+ is used as the alkaline cation, the (002) peak is very broad and hardly detected. However, the reflection becomes more intense and narrower when a low amount of K^+ ions ($K^+/GMP = 0.39{:}1$, slightly higher than the stoichiometric amount for the intertetramer position, that is, $K^+/GMP = 0.25{:}1$) is incorporated in the synthesis mixture. Further increases in the K^+ concentration ($K^+/GMP = 5.1{:}1$) in the synthesis mixture do not cause the peak to increase in intensity. The same trend is found when looking at the (001) reflection, which suggests that the intertetramer positions are occupied by K^+ ions.

Attempts to eliminate the GMP template by either extraction or calcination resulted in the collapse of the mesostructure. To improve the stability of the mesostructure, the synthesis mixture was hydrothermally treated at 100 °C in an autoclave. The XRD pattern of the resulting solid after 4 days (denoted *h*NGM-1) still exhibits a pattern that can be indexed within hexagonal symmetry (Figure 2). Mesoscale reflections as high as (140) are clearly visible, and with unit cell parameters ($a = 38.5$ Å and $c = 3.4$ Å) larger than that of the *a*NGM-1 sample prepared at room temperature. A change in the relative intensities of the mesoscale reflections is also observed, as a result of the more condensed silica wall. Chemical analysis of the sample led to a composition of $4\,GMP : 8.86\,SiO_{3/2}(CH_2)_3NH_2 : 31.18\,SiO_2 : 0.28\,Na_2O : 0.61\,K_2O : 48.31\,H_2O$ per tetramer, thereby revealing that the increase in the unit cell accompanies an increase in the incorporated silica (see Figures S1–S3 in the Supporting Information). Solvent extraction prior to calcination yielded ordered mesoporous solids, with XRD patterns (see Figure S5 in the Supporting Information) showing sharp peaks in the mesoscale range and lacking the reflections related to ordering on the atomic scale. The unit cell parameters are $a = 37.6$ Å and $a = 34.2$ Å for the extracted and calcined solids, respectively. Thus, the hydrothermal treatment is necessary to produce robust structures that can sufficiently undergo template extraction and calcination.

The ^{1}H NMR spectra of the hydrothermally treated and extracted samples (dissolved in $NaOD/D_2O$) show only the three methylene signals from the aminopropyl group, thus indicating an adequate extraction of the template. The

addition of tetraethylammonium bromide as an internal standard led to a ratio of 3.35 mmol of amines per gram of SiO_2 (1/5 silicon atoms are bound to an amine group). Nitrogen adsorption isotherms (Figure 3) were conducted on the solvent-extracted and calcined NGM-1 mesoporous material (denoted *e*NGM-1 and *c*NGM-1). By taking into account

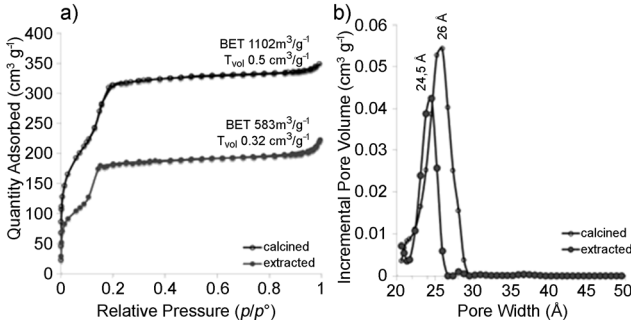

Figure 3. a) Nitrogen sorption isotherms for calcined and extracted samples of *e*NGM-1 and *c*NGM-1, and b) corresponding pore size distribution curves.

the surface area of the extracted sample (583 $m^2 g^{-1}$), a value of 1 amine moiety every 34 $Å^2$ was obtained, which constitutes a high functionalization coverage. The nitrogen isotherm profiles are consistent with a type IV curve, albeit with a low pressure capillary condensation step occurring between 0.1 and 0.2 (P/P^o) and the absence of any hysteresis effect. This is indicative of a small mesopore size, which is confirmed from pore size distribution curves, which are centered at 24.5 and 26.0 Å for the *e*NGM-1 and *c*NGM-1 samples, respectively. Almost a doubling of the surface area to 1102 $m^2 g^{-1}$ is observed upon calcination, because of the rougher surface resulting from the thermal treatment and the removal of the propylamine moieties.

Scanning electron microscopy (SEM) images show the mesoporous *h*NGM-1 particles to be composed of faceted trigonal and ditrigonal prisms and rods (Figure 4a, see also Figure S7 in the Supporting Information), which is suggestive of a lower symmetry structure than the assumed hexagonal system. Transmission electron microscopy images (Figure 4b, see also Figure S7 in the Supporting Information) of *h*NGM-1 show a well-ordered pore arrangement. The lattice parameter calculated from electron diffraction patterns on the basis of a hexagonal unit cell is $a = 32.3$ Å, which is smaller than that measured from the XRD patterns shown in Figure 2 (38.5 Å). Transmission electron microscopy (TEM) images recorded parallel to the pore direction show a dark contrast within the pores. Further analysis is necessary to determine the origin of this contrast. However, images recorded under a variety of focus conditions and corrected for contrast transfer function effects[15] show similar dark contrast within the pores (Figure 4c, see also Figure S7 in the Supporting Information). Potential density maps modeled from this analysis (Figure 4d) show an area of higher density in the center of the channel space. Along this zone axis, there is apparent sixfold symmetry, as observed from simulated Fourier Transform (FT) diffractograms or from selected-

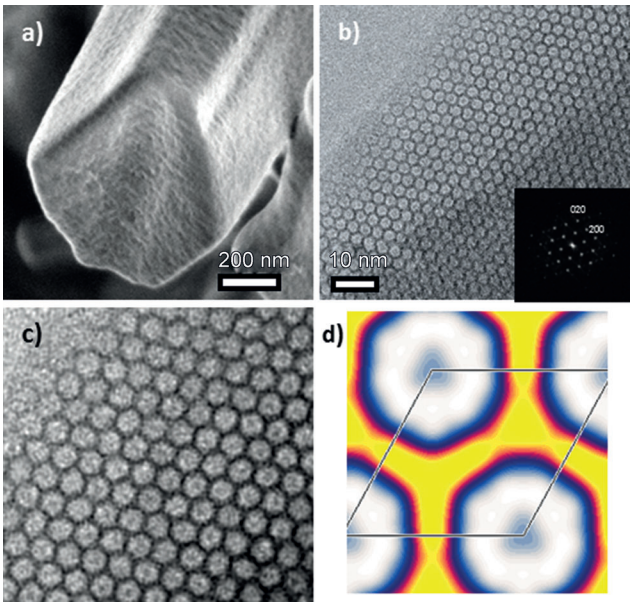

Figure 4. Scanning and transmission electron microscopy images recorded parallel to the *c*-axis of a *h*NGM-1 particle showing: a) ditrigonal faceting, and b) the well-ordered arrangement of pores with dark contrast within the pores. The inset in (b) shows the indexed Fourier transform (FT) diffractogram of the image shown. c) The contrast transfer function (CTF) corrected image reconstructed from a through focus series is shown together with d) the potential density map along the [001] direction (see Figure S7 in the Supporting Information for more details). Color gradient: white→blue→red→yellow shows areas of low→high density.

area diffraction patterns (SAED). However, as noted from the SEM images, the crystal habit of the particles is varied and particles corresponding to a trigonal system are evident. Comparison of the phase residual information of diffraction spots as well as the amplitude relationship between specific reflections leads to a *p*3m1 symmetry along the [001] direction (see Figure S7 in the Supporting Information). However this is not a sufficient difference to assign a trigonal crystal class. Tilting series and images recorded along other orientations (see Figure S7 in the Supporting Information) show only two additional zone axes with *p*1 symmetry. No general reflection conditions could be observed from diffractograms recorded along any orientation. Note that a trigonal pattern cannot be rejected on the basis of the hexagonal honeycomb pattern. Furthermore, nonresonant X-ray diffraction cannot distinguish between trigonal and hexagonal symmetries, and hence the XRD pattern can be indexed on the basis of a hexagonal or trigonal symmetry. Hence, it is not possible to unequivocally assign a trigonal crystal class and thus we tentatively assigned a three-dimensional space group with *P*6 symmetry as that with the highest symmetry.

Fourier transform diffractograms recorded on a number of crystals along the [001] direction show the appearance of a diffuse scattering pattern with a Star of David motif (Figure 5 and see Figure S8.3 in the Supporting Information) consistent with the crystal lattice. Similar motifs have been encountered in isotactic polymers with trigonal symmetries as well as in inclusion compounds of *n*-alkanes in urea, where the

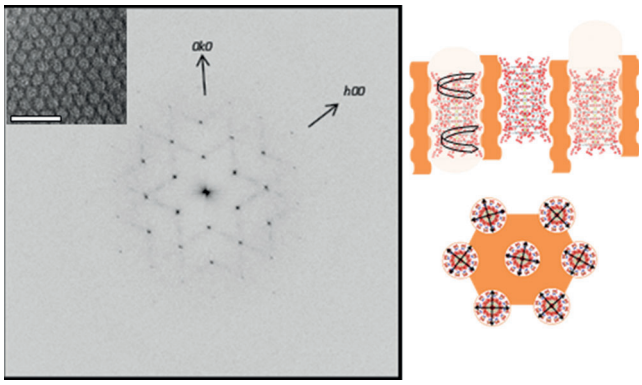

Figure 5. FT diffractogram recorded on a particle of *h*NGM-1 (the inset shows a portion of the image used, scale bar = 10 nm) along the [001] orientation, showing prominent diffuse scattering between specific reflections. Possible models of the template rotation along the pores and of the independent arrangement of tetramers in each channel are also shown (right), which could induce the diffuse scattering pattern observed.

host and guest substructures have a different dimensionality, as in the 3D-ordered urea-host framework and a predominately 1D guest structure of the alkane chains.[16,17] Similar patterns have recently been observed in mesoporous materials prepared with chiral surfactants and possessing 2D rectangular (*p2gg*) pore systems, accounted for by elliptical pore shapes clearly visible through TEM imaging.[18] In the case of NGM-1, diffuse scattering is also observed along the [001] direction, that is, parallel to the channels containing the tetrameric GMP template. The position of the diffuse scattering is commensurate with the reciprocal lattice of the silica framework since it occurs along specific lattice reflections. Furthermore, masking the diffraction spots associated with the silica lattice on FT diffractograms and performing an inverse Fourier Transform to retrieve the image (data not shown) has little effect on the image contrast and pattern. The diffuse scattering patterns observed can be explained in terms of three factors: 1) helical rotation of the tetramers in which the two G quartets ($G4_N$ and $G4_S$ type) are twisted by 30° with respect to each other (60° with respect to the next repeat unit) and stacked in a right-handed fashion with an axial rise of 3.4 Å along the pore direction;[5] 2) corrugation of the silica surface as a result of molecular imprinting; and 3) independent tetramer positions on each pore channel (see Figure 5 inset).[17] Modeling of the diffuse scattering may yield fine structural details of the GMP stacking arrangement and its chirality within the pores. The latter is confirmed by circular dichroism measurements of *h*GMP-1 (see Figure S8 in the Supporting Information), which are consistent with previously reported spectra for a Na_2(5′-GMP) in self-assembled G quartets with *N*- and *S*-type tetramers (antiparallel arrangement).[1,19]

Barboui and co-workers recently characterized a mesostructured material made by the condensation of guanine-siloxane monomers, termed G_{Si}, in the absence of any additional silica source.[20] The authors conclude that supramolecular assembled G_{si} units form hexagonal *p*6mm symmetries, with chiral transcription from the template to the silica wall promoted through the rigid covalent linker between the silica and G quartet. Moreover, the assignment of a 2D planar space group is somewhat surprising due to the presence of clear atomic order along the *c*-direction within the prepared G_{si} structure. For both these mesostructured materials (G_{si} and NGM-1), a nonchiral space groups is chosen on the basis of the available information.

The present results show that well-ordered and stable mesoporous silica may be easily prepared using nucleotides capable of forming supramolecular quadruplex structures in solution. The use of APES creates an additional supramolecular interaction that allows the replication/transcription of the GMP columns into the inorganic silica matrix. The observation of high-angle X-ray diffraction peaks allows the template to be included in the mesoscale structural analysis, and the diffuse scattering observed by electron microscopy shows a distinct relationship between the mesoscale order and chiral tetramer stacking. The chirality of the template within the pores is confirmed by circular dichroism. Mesotructured NGM-1 possesses a lower symmetry than the expected hexagonal symmetry, thus indicating an anisotropic columnar packing arrangement. This report demonstrates a promising route to develop a family of nucleotide hybrid materials, based on the GMP tetramer motif as well as other nucleic acid systems.

Experimental Section

The synthesis of NGM-1 materials was carried out using the chemicals as purchased and without further purification. Initially, guanosine 5-monophosphate disodium salt hydrate (300 mg, Aldrich, from yeast, ≥ 99 %, determined by ^{1}H NMR spectroscopy to be $Na_2GMP{\cdot}7H_2O$) were dissolved in H_2O (10.5 mL, milliQ) in a teflon vessel. KCl (130.2 mg, Aldrich) was added, and the mixture left to stir (200 rpm) for 1 h. The stirring rate was increased to 400 rpm before addition of aminopropyltriethoxysilane (386 μL, APES) followed by HCl (37 %; 135.5 μL). After one minute, tetraethyl orthosilicate (552 μL, TEOS) was added and left under stirring for 2 h with the lid on. After this, solid (350 mg) was filtered off and characterized. This solid was named *a*NGM-1 to denote the as-synthesized material. The overall molar composition was 1 $GMPNa_2$: 2.93 APES : 4.4 TEOS : 2.91 HCl : 3.1 KCl : 1054 H_2O. When hydrothermal treatment was conducted, the synthesis mixture was placed, before filtration, in an autoclave and heated at 100 °C for four days. After filtration, solid (351 mg) was obtained. This solid was named *h*NGM-1 to denote the hydrothermal treatment. The hydrothermally treated sample (*h*NGM-1, 150 mg) was extracted in a solution of ethanol (13.5 mL) and HCl (37 %, 1.5 mL). After stirring the mixture for 20 h at room temperature, the remaining solid was obtained by filtration. The extracted sample (denoted *e*NGM-1) was calcined in air at 550 °C for 3 h and was denoted *c*NGM-1. The XRD patterns and adsorption isotherms of *e*NGM-1 and *c*NGM-1 are shown in Figures S4 and S5 in the Supporting Information.

X-ray diffraction (XRD) patterns were recorded on a Bruker D8 Advance X-ray diffractometer with a $Cu_{K\alpha}$ anode ($\lambda = 0.1542$ nm) operating at 40 kV and 30 mA.

For full details of the characterization equipment used, please see the Supporting Information.

Received: July 14, 2014
Published online: September 11, 2014

Keywords: chirality · electron microscopy · hybrid materials · mesoporous materials · self-assembly

[1] J. T. Davis, G. P. Spada, *Chem. Soc. Rev.* **2007**, *36*, 296 – 313.
[2] W. Guschlbauer, J.-F. Chantot, D. Thiele, *J. Biomol. Struct. Dyn.* **1990**, *8*, 491 – 511.
[3] D. Monchaud, M. P. Teulade-Fichou, *Org. Biomol. Chem.* **2008**, *6*, 627 – 636.
[4] a) S. Mann, *Angew. Chem. Int. Ed.* **2013**, *52*, 155 – 162; *Angew. Chem.* **2013**, *125*, 166 – 173; b) B. Liu, L. Han, S. Che, *Angew. Chem. Int. Ed.* **2012**, *51*, 923 – 927; *Angew. Chem.* **2012**, *124*, 947 – 951; c) A. R. Hilgenbrink, P. S. Low, *J. Pharm. Sci.* **2005**, *94*, 2135 – 2146.
[5] a) W. Gang, I. C. M. Kwan, *J. Am. Chem. Soc.* **2009**, *131*, 3180 – 3182; b) T. J. Pinnavaia, H. T. Miles, E. D. Becker, *J. Am. Chem. Soc.* **1975**, *97*, 7198 – 7200.
[6] J. T. Davis, *Angew. Chem. Int. Ed.* **2004**, *43*, 668 – 698; *Angew. Chem.* **2004**, *116*, 684 – 716.
[7] a) S. Che, A. E. Garcia-Bennett, K. Yokoi, K. Sakamoto, H. Kunieda, O. Terasaki, T. Tatsumi, *Nat. Mater.* **2003**, *2*, 801 – 805; b) A. E. Garcia-Bennett, N. Kupferschmidt, Y. Sakamoto, S. Che, O. Terasaki, *Angew. Chem. Int. Ed.* **2005**, *44*, 5317 – 5322; *Angew. Chem.* **2005**, *117*, 5451 – 5456.
[8] a) R. Atluri, N. Hedin, A. E. Garcia-Bennett, *J. Am. Chem. Soc.* **2009**, *131*, 3189 – 3192; b) R. Atluri, N. M. Iqbal, Z. Bacsik, N. Hedin, L. A. Villaescusa, A. E. Garcia-Bennett, *Langmuir* **2013**, *29*, 12003 – 12012.
[9] H. Qiu, J. Xiea, S. Che, *Chem. Commun.* **2011**, *47*, 2607 – 2609.
[10] J. Sauer, F. Marlow, F. Schueth, *Phys. Chem. Chem. Phys.* **2001**, *3*, 5579 – 5584.
[11] K. Kanie, M. Nishii, T. Yasuda, T. Taki, S. Ujiieb, T. Kato, *J. Mater. Chem.* **2001**, *11*, 2875 – 2886.
[12] P. Mariani, F. Spinozzi, F. Federiconi, H. Amenitsch, L. Spindler, I. Drevensek-Olenik, *J. Phys. Chem. B* **2009**, *113*, 7934 – 7944.
[13] M. Khaled, C. L. Krumdieck, *Biochem. Biophys. Res. Commun.* **1985**, *130*, 1273 – 1280.
[14] J.-L. Mergny, A. De Cian, A. Ghelab, B. Sacca, L. Lacroix, *Nucleic Acids Res.* **2005**, *33*, 81 – 94.
[15] W. Wann, S. Hovmöller, X. Zou, *Ultramicroscopy* **2012**, *115*, 50 – 60.
[16] D. L. Dorset, M. P. McCourta, S. Kopp, M. Schumacher, T. Okihara, B. Lotz, *Polymer* **1998**, *39*, 6331 – 6337.
[17] a) T. Weber, H. Boysen, F. Frey, *Acta Crystallogr. Sect. B* **2000**, *56*, 132 – 141; b) T. R. Welberry, S. C. Mayo, *J. Appl. Crystallogr.* **1996**, *29*, 353 – 364.
[18] H. Qiu, Y. Sakamoto, O. Terasaki, S. Che, *Adv. Mater.* **2008**, *20*, 425 – 429.
[19] M. Panda, J. A. Walmsley, *J. Phys. Chem. B* **2011**, *115*, 6377 – 6383.
[20] C. Arnal-Hérault, A. Banu, M. Barboiu, M. Michau, A. Lee, *Angew. Chem. Int. Ed.* **2007**, *46*, 4268 – 4272; *Angew. Chem.* **2007**, *119*, 4346 – 4350.

